The use of random forests to classify amyloid brain PET

Katherine Zukotynski, MD, University of Toronto, Toronto and McMaster University, Hamilton, ON, Canada
Vincent Gaudet, PhD, University of Waterloo, Waterloo, ON, Canada
Phillip H. Kuo, MD, PhD, University of Arizona, Tucson, AZ
Sabrina Adamo, HBSc, Sunnybrook Research Institute, Toronto, ON, Canada
Maged Goubran, PhD, Sunnybrook Research Institute, Toronto, ON, Canada
Christopher Scott, BScH, Sunnybrook Research Institute, Toronto, ON, Canada
Christian Bocti, MD, Université de Sherbrooke, Sherbrooke, QC, Canada
Michael Borrie, MB ChB, Western University, London, ON, Canada
Howard Chertkow, MD, Jewish General Hospital, Montreal, QC, Canada
Richard Frayne, PhD, Hotchkiss Brain Institute, University of Calgary, Calgary, AB, Canada and Seaman Family MR Research Centre, Foothills Medical Centre, Calgary, AB, Canada
Robin Hsiung, MD, University of British Columbia, Vancouver, BC, Canada
Robert Laforce, Jr., MD, PhD, Université Laval, Québec, QC, Canada
Michael D. Noseworthy, PhD, McMaster University, Hamilton, ON, Canada
Frank S. Prato, PhD, Western University, London, ON, Canada
Demetrios J. Sahlas, MD, McMaster University, Hamilton, ON, Canada
Eric E. Smith, MD, Hotchkiss Brain Institute, University of Calgary, Calgary, AB, Canada
Vesna Sossi, PhD, University of British Columbia, Vancouver, BC, Canada
Alex Thiel, MD, Jewish General Hospital, Montreal, QC, Canada
Jean-Paul Soucy, MD, Montreal Neurological Institute, Montreal, QC, Canada
Jean-Claude Tardif, MD, Montreal Heart Institute, Montreal, QC, Canada
Sandra E. Black, MD, Department of Medicine (Neurology), Sunnybrook Health Sciences Centre and Sunnybrook Research Institute, University of Toronto, Toronto, ON, Canada

Name and address for correspondence:
Katherine Zukotynski
Address: McMaster University, 1200 Main St. W., Rm. 1P11, Hamilton, ON L8P 3Z5 Canada
Fax: 905-577-1443
Phone: 647-926-0194
Email: katherine.zukotynski@utoronto.ca

Short title: Random forests and amyloid brain PET

Acknowledgement: We are grateful for funding from CIHR MITNEC C6 (mitnec.ca), from the Linda C Campbell Foundation and for in-kind support from Lilly-Avid Radiopharmaceuticals who generously provided the amyloid ligand. Also, we wish to acknowledge S. Mathotaarachchi and P. Rosa-Neto at McGill University for their help with the MINC-based image processing pipeline.

The content of this paper was presented at the 2019 ACNM Meeting in Palm Springs, CA

The use of random forests to classify amyloid brain PET

Abstract

Purpose: To evaluate random forests (RF) as a supervised machine learning algorithm to classify amyloid brain PET as positive or negative for amyloid deposition, and identify key regions of interest (ROI) for stratification.

Materials and methods: The dataset included 57 baseline ^{18}F-Florbetapir (Amyvid, Avid) brain PET scans in participants with severe white matter disease, presenting with either transient ischemic attack/ lacunar stroke or mild cognitive impairment from early Alzheimer's disease, enrolled in a multi-center prospective observational trial. Scans were processed using the MINC toolkit to generate standardized uptake values ratios (SUVR), normalized to cerebellar grey matter and clinically read by two nuclear medicine physicians with interpretation based on consensus (35 negative, 22 positive). SUVR data and clinical reads were used for supervised training of an RF classifier programmed in Matlab.

Results: A 10,000 tree RF, each tree using 15 randomly selected cases and 20 randomly selected features (SUVR per ROI), with 37 cases for training and 20 cases for testing, had sensitivity=86% (95% confidence interval (CI): 42-100%), specificity=92% (CI: 64-100%), and classification accuracy=90% (CI: 68-99%). The most common features at the root node (key regions for stratification) were: 1) left posterior cingulate (1039 trees), 2) left middle frontal gyrus (1038 trees) 3) left precuneus (857 trees), 4) right anterior cingulate gyrus (655 trees), and 5) right posterior cingulate (588 trees).

Conclusions: RFs can classify brain PET as positive or negative for amyloid deposition and suggest key clinically relevant, regional features for classification.

Keywords: Amyloid, brain PET, dementia, white matter disease, machine learning, random forest

Introduction

Mild cognitive impairment (MCI) is defined as cognitive decline greater than expected for age but not interfering with the activities of daily living [1]. It is estimated that 10-15% of individuals with MCI annually progress to dementia along a defined temporal course [2,3]. Dementia refers to a host of progressive neurodegenerative conditions resulting in loss of cognitive function sufficient to disrupt daily living activities [4]. Alzheimer's disease (AD), comprising amyloid plaques and tau tangles, is a frequent pathology in autopsies, commonly co-morbid with other proteinopathies and vasculopathies [5]. While the AD clinical syndrome relates, in part, to beta-amyloid (Aβ) protein deposition [6,7], tau progression along functional neural networks is thought to better track the gradual decline in episodic memory followed by language, visuo-spatial and executive difficulties [8].

The diagnosis of MCI and AD is based on clinical evaluation; however, imaging plays a key supportive role. Computed tomography (CT) and magnetic resonance imaging (MRI) are often used to exclude vascular lesions or masses, detect cerebral atrophy and monitor disease severity. Positron emission tomography (PET) can detect amyloid deposition, among other biomarkers of disease. ^{18}F-Florbetapir (Amyvid, Lilly) is a PET radiopharmaceutical that has high sensitivity (87%), specificity (95%) and accuracy (90%) for detecting moderate-to-frequent cortical amyloid plaque based on neuropathology at autopsy [9]. Clinically, ^{18}F-Florbetapir brain PET scans are classified as positive or negative for amyloid deposition based on an overall subjective interpretation, although quantitation of radiotracer uptake permits a more granular evaluation and could potentially pinpoint key regions of the brain for classification. While amyloid deposition can be seen in both normal and demented subjects [10-12], the negative predictive value (NPV) of amyloid PET/CT is high (i.e. if the scan is negative, the likelihood of AD is low) [13].

Machine learning (ML) algorithms vary widely in their complexity, approach, and applications to medical imaging [14]. A random forest (RF) [15] is a supervised ML algorithm that consists of a collection of decision trees, where a decision tree (**Figure 1**) is a graphical structure that starts at a root node and branches out, possibly in several steps, towards leaf nodes that indicate classification outcomes. At each branch point, a feature is inspected and a decision is made to branch left or right, based on a trained condition. For example, whether the feature value is less than or greater than a threshold value that is chosen to separate training data into two classes with greatest classification accuracy. Leaf nodes are labeled with classes (e.g., negative or positive), and indicate the final outcome of a tree. To train an RF, each tree is constructed using a randomly selected subset of training cases from the complete dataset of cases and a randomly selected subset of features from the complete set of features. After training, each new case is evaluated using the RF. Since each tree in the RF is built from a random subset of cases and features, it reflects a subsample of the entire training space. For each new case being evaluated, unanimity of decisions among all trees in the RF is uncommon. The final decision of an RF is the class that is most common after inspection of all trees. There are several advantages to using an RF for classifying imaging data. For example, RFs can provide insight on decisions through extracting features that commonly appear at the root node of a tree, e.g. features that are important for a classification outcome.

In this paper, we explore the use of RFs to: 1. classify amyloid brain PET scans as positive or negative for amyloid deposition in a patient population with significant vascular disease, and 2. identify key regions of the brain for scan classification.

Materials and Methods

Fifty-seven subjects with severe white matter disease, presenting with mild cognitive impairment from early AD or transient ischemic attack/ lacunar stroke, were enrolled in a multi-center prospective observational trial through 9 participating sites as part of the C6 project in the Medical Imaging Network of Canada [16-18]. While accrual to this study is ongoing, these 57 subjects were the full patient cohort at the time of our analysis. Of these 57 subjects, 38 were recruited from participating memory clinics and 19 were recruited from stroke prevention clinics. Inclusion criteria included a Mini Mental Status Examination (MMSE) score > 20, among other factors; significant medical or other neurological conditions were cause for exclusion, among other factors [17,18]. Each participant had a ^{18}F-Florbetapir brain PET scan as well as a quantitative 3T MRI including 3D T1, PD/T2, FLAIR, Gradient Echo, DTI and resting state fMRI acquisitions.

The ^{18}F-Florbetapir brain PET scans were obtained using scanners available at participating sites; consistency of PET data across sites was maintained by adherence to a standard quality assurance program and use of a common imaging protocol, including the main ADNI2 structural protocol [19]. Specifically, the imaging protocol stipulated that 370 MBq (10 mCi +/- 10%) ^{18}F-Florbetapir was to be administered intravenously followed by 20 minutes of dynamic imaging approximately 50 minutes post radiopharmaceutical administration consisting of four-5 minute acquisitions with attenuation and scatter correction. All imaging was transferred to a central site for review of quality and protocol adherence. The brain PET scans were clinically interpreted as positive or negative for amyloid deposition by two dual certified nuclear medicine physicians/ radiologists blinded to each other's opinion and using MIM software (MIM Software Inc., Cleveland Ohio) with disagreement resolved through unblinded discussion and consensus. To obtain quantitative data, all brain PET scans were subsequently processed using a pipeline based on the MINC toolkit [20] (**Figure 2**). Where possible, the four 5-minute image acquisitions were averaged and then blurred to a common 7-mm full width half maximum (FWHM) to account for differences in camera resolution across sites. PET images were subsequently registered to the Montreal Neurological Institute template space using the patient MRI as an intermediate step. In template space, unique masks were used to calculate standardized uptake value ratios (SUVRs) for brain regions of interest (ROIs), normalized to cerebellar grey matter. The atlas used for the ROIs included 58 individual brain ROIs, as well as a composite ROI based on the prefrontal, orbitofrontal, parietal, temporal, anterior cingulate, and posterior cingulate/ precuneus regions (referred to as the Jack mask, often affected in AD) [21]. Thus, each brain PET scan was associated with 59 ROIs or a total of 59 feature values.

The complete dataset of 57 brain PET scans was randomly divided into a training set with 37 scans and a testing set with 20 scans (**Table 1**). An RF with 10,000 trees, 15 randomly selected cases (out of 37 training scans), and 20 randomly selected feature values (out of 59 feature values) for each tree, was programmed in Matlab and trained with the goal of classifying brain PET scans as negative versus positive for amyloid deposition. Thus, the SUVRs and clinical reads were used for supervised training of our RF classifier that we programmed, with two objectives: 1. To evaluate classification performance, and 2. To determine which brain ROIs have the greatest importance for scan classification.

Results

Of the 57 subjects, 27 were female and 30 were male; age range was 57-91 years (median 76 years, mean 76.6 years, standard deviation 8.6). All participants had significant white matter disease, with a range in white matter hyperintensity volume of 8.2-103.7cm^3 (median 26.3 cm^3, mean 34.7 cm^3, standard deviation 23.4 cm^3). Based on clinical interpretation, 35 brain PET scans were negative for amyloid deposition and 22 were positive. Based on the quantitative analysis, the SUVR over the Jack mask range was 0.68-2.49 (median 1.44, mean 1.49, standard deviation 0.34).

The RF classified scans as negative or positive for amyloid deposition using SUVR data, with 90% accuracy (95% confidence interval (CI) using exact Clopper-Pearson method: 68-99%), sensitivity 86% (CI: 42-100%) and specificity 92% (CI: 64-100%) where the clinical scan interpretation served as the gold standard. The confusion matrix summarizing the RF classification results is given in **Table 2**. The 10 most common ROIs at the root nodes of the 10,000 trees (most relevant for scan classification) were the: 1. Left posterior cingulate (1039 trees), 2. Left middle frontal gyrus (1038 trees), 3. Left precuneus (857), 4. Right anterior cingulate gyrus (655 trees), 5. Right posterior cingulate (588 trees), 6. Right precuneus (408 trees), 7. Left anterior cingulate gyrus (342 trees), 8. Right gyrus rectus (319 trees), 9. Left gyrus rectus (299 trees) and 10. Right middle temporal gyrus (270 trees) (**Table 3**). If features were to be assigned randomly to the root nodes in a forest (no training), we would expect that any individual feature would be at the root node of approximately 10,000 / 59 = 169 trees. In other words, the most common feature (left posterior cingulate) in the trained forest was used in 6 times more trees than would be expected by random chance, indicating strong relevance. The key ROIs identified by the RF on a surface projection of the brain are illustrated in **Figure 3**.

The number of trees in the RF that returned negative and positive classifications for each test case is provided in **Table 4**. The relative frequency of positive versus negative classifications suggests an indication of the confidence in the final decision. We observe that the decisions for the two false classifications were weaker than in the majority of true classifications: 4,183 trees returning a negative (correct) decision versus 5,817 returning a positive (incorrect) decision for the false positive case, and 5,426 trees returning a negative (incorrect) decision versus 4,572 trees returning a positive (correct) decision for the false negative case. For true positive and true negative cases, the average number of trees returning the correct decision was 7,420, and the average number of trees returning the incorrect decision was only 2,580.

Cross-validation was performed by running 30 instances of the RF algorithm using the same parameters (15 cases per tree, 20 features per tree, and 10,000 trees) but where the data set was randomly re-split into a different breakdown of 37 training and 20 test cases. Overall, this resulted in 85% sensitivity, 89% specificity, and 87% classification accuracy, justifying that our initial results were close to the norm.

Discussion

Amyloid deposition and vascular disease are among the most common causes of dementia and often co-exist. Although the diagnosis of MCI and AD is made clinically, often based on a combination of a clinical examination and neuropsychological assessment, there has been a recent push to include imaging. Indeed, in 2016, Jack et al. proposed to use a descriptive “A/T/N” system in subjects with

suspected dementia to avoid the lack of consensus in clinical diagnostic schemes. In this system "A" refers to amyloid positivity (on amyloid PET or CSF $A\beta_{42}$), "T" refers to tau positivity (on tau PET or CSF phospho tau) and "N" refers to neurodegeneration or neuronal injury (on ^{18}F-FDG PET, MRI or CSF total tau) [22]. Also, the National Institute on Aging and Alzheimer's Association (NIA-AAA) research framework suggested AD be defined by its underlying pathologic processes using a combination of biomarkers such as Aβ deposition, pathologic tau and neurodegeneration, irrespective of clinical manifestations [23]. Although this approach may be less subjective than a combination of signs and symptoms, it is likely to be more expensive with difficulties in practical implementation. To date, establishing consensus on the best way to assess cognitive impairment remains a topic of heated debate. Nevertheless, there has been a push to include MRI and amyloid brain PET in the evaluation of subjects with suspected dementia.

Imaging features may be predictive of clinical status in subjects with cognitive impairment. For example, de Vos et al. showed that brain MRI features including cortical thickness, grey matter density and hippocampal shape, among others, could discriminate subjects with AD from healthy controls and that a combination of features was more accurate than any single feature [24]. Further, MRI features have been combined with features from other imaging modalities such as PET in the search for predictive biomarkers of disease [25]. Recently, there has been an explosion in the use of ML algorithms including RFs for the analysis of imaging data. Often the goal of the ML algorithm is to use imaging features to predict clinical status. For example, Dimitriadis et al. quantified the prediction accuracy of brain MRI features using an RF to discriminate among health controls, early mild MCI, late MCI and AD [26]. A systematic review by Sarica et al. suggested RFs can be successfully used with neuroimaging data to predict AD [27]. The best accuracies (approximately 90%) were obtained when RFs were trained to distinguish AD from healthy controls using multi-modality data. Although this dropped slightly (approximately 80%) for distinguishing MCI from healthy controls, it improved when additional non-imaging data such as age or the results of cognitive assessment were included.

Our results show that a 10,000-tree RF using 15 randomly selected cases for each tree, 20 randomly selected ROIs and a training set of 37 scans can stratify ^{18}F-Florbetapir brain PET scans as negative or positive for amyloid deposition with 90% accuracy (CI: 68-99%). It was difficult to determine why the RF classification of certain cases was discordant with the clinical interpretation. Out of 20 test cases (Table 3), there was only one false positive case; case 4 was from a stroke clinic, with SUVR over the Jack mask of 1.74, and white matter hyperintensity volume of 22.3cm^3. There was also only one false negative case; case 20 was from a memory clinic, with SUVR over the Jack mask of 1.50, and white matter hyperintensity volume of 22.9cm^3. Case 18 was a true negative case but with very similar numbers of trees indicating negative and positive outcomes; in this case, the patient was from a stroke clinic, SUVR over the Jack mask was 1.71, and the white matter hyperintensity volume of 18.5cm^3.

The ROIs that were key for scan classification using this RF are consistent with those that are known to be associated with amyloid pathology in subjects with AD. Both imaging and pathologic studies have suggested that the cerebral cortical regions in which amyloid deposition is commonly found in subjects with AD include the: frontal lobe, parietal lobe, temporal lobe, precuneus and anterior and posterior cingulate gyrus regions consistent with our findings [8,28]. It has also been suggested that amyloid accumulation preferentially starts in the precuneus, medial orbitofrontal and posterior cingulate

cortices [29] and that the affected cortical regions may be part of the default mode network whose disruption contributes to memory impairment [30].

The main limitations of this study are the method of data labeling and the small sample size. Given that the inherent accuracy of clinical scan interpretation is approximately 90% [9], there could be errors of interpretation by the imaging experts. Also, pathology was not available for confirmation and a larger group of imaging experts blinded to each other's opinion would have been time intensive and was beyond the scope of this feasibility study. Further, given the small size of our dataset, we could not effectively create a validation dataset of brain PET scans. Normally, a validation dataset can be used to explore hyperparameters such as the number of trees, number of cases per tree, and number of ROIs per tree used in the creation of the RF, possibly improving the results of the RF. However, it is noteworthy that even in this sample of amyloid positive cases with severe white matter disease, key hubs in the default mode network are detected with a hypothesis-free methodology.

Conclusions

This preliminary investigation shows that random forests can classify ^{18}F-Florbetapir brain PET as positive or negative for amyloid deposition. This approach confirmed important brain ROIs (features) used for classification that include key nodes, part of the default node network, where amyloid deposition preferentially begins in the brain.

References

1. Gauthier S, Reisberg B, Zaudig M, et al. Mild cognitive impairment. Lancet. 2006; 367:1262–1270.
2. Jack CR Jr., Knopman DS, Jagust WJ, et al. Hypothetical model of dynamic biomarkers of the Alzheimer's pathological cascade. Lancet Neurol. 2010; 9:119–128.
3. Jack CR Jr. Alzheimer disease: new concepts on its neurobiology and the clinical role imaging will play. Radiology. 2012; 263:344–361.
4. Goodman RA, Lochner KA, Thambisetty M, et al. Prevalence of dementia subtypes in US Medicare fee-for-service beneficiaries, 2011-2013. Alzheimers Dement. 2017;13(1):28-37.
5. Kapasi A, DeCarli C and Schneider JA. Impact of multiple pathologies on the threshold for clinically overt dementia. Acta Neuropathol. 2017; 134(2):171-186.
6. Shinohara M, Fujioka S, Murray M, et al. Regional distribution of synaptic markers and APP correlate with distinct clinicopathological features in sporadic and familial Alzheimer's disease. Brain. 2014; 137:1533-1549.
7. Crews L, Masliah E. Molecular mechanisms of neurodegeneration in Alzheimer's disease. Hum Mol Genet. 2010;19(R1): R12-R20.
8. Braak H and Braak E. Neuropathological stageing of Alzheimer-related changes. Acta Neuropathol. 1991; 82:239-259.
9. Clark CM, Pontecorvo MJ, Beach TG, et al. Cerebral PET with florbetapir compared with neuropathology at autopsy for detection of neuritic amyloid-beta plaques: a prospective cohort study. Lancet Neurol. 2012; 11:669 –78.
10. Sojkova J, Zhou Y, An Y, et al. Longitudinal patterns of β-amyloid deposition in nondemented older adults. Arch Neurol. 2011;68(5):644-649.

11. Rowe CC, Villemagne VL. Brain amyloid imaging. J Nucl Med. 2011; 52:1733–1740.
12. Rowe CC, Ng S, Ackermann U, et al. Imaging beta-amyloid burden in aging and dementia. Neurology. 2007; 68:1718–1725.
13. Nordberg A, Carter SF, Rinne J, et al. A European multicentre PET study of fibrillar amyloid in Alzheimer's disease. Eur J Nucl Med Mol Imaging. 2013; 40:104–114.
14. Uribe CF, Mathotaarachchi S, Gaudet VC, et al. Part 1: Introduction to Machine Learning in the Nuclear Medicine Context. J Nucl Med. 2019. [Epub ahead of print]
15. Ho TK. Random Decision Forests. Proc Int Conf Document Analysis and Recognition, Montreal, QC. 1995:278–282.
16. Fazekas F, Chawluk JB, Alavi A, et al. MR signal abnormalities at 1.5T in Alzheimer's dementia and normal aging. AJR Am J Roentgenol. 1987; 149(2):351-356.
17. MITNEC Theme C: Imaging Trials in Neurology. http://www.mitnec.org/ (accessed April 8, 2019)
18. Amyloid and Glucose PET Imaging in Alzheimer and Vascular Cognitive Impairment Patients With Significant White Matter Disease (MITNEC C6): NCT02330510. www.clinicaltrials.gov (accessed April 8, 2019)
19. Petersen R, Weiner M. ADNI 2 Procedures Manual. 2008. http:// adni.loni.usc.edu/wp-content/uploads/2008/07/adni2-procedures- manual.pdf (accessed April 1, 2019)
20. MINC Toolkit. McConnell Brain Imaging Centre. http://www.bic.mni.mcgill.ca/ServicesSoftware/MINC (accessed March 31, 2019)
21. Jack CR Jr., Lowe VJ, Senjem ML, et al. ^{11}C PiB and structural MRI provide complementary information in imaging of Alzheimer's disease and amnestic mild cognitive impairment. Brain. 2008; 131:665-680.
22. Jack CR, Jr., Bennett DA, Blennow K, et al. A/T/N/: An unbiased descriptive classification scheme for Alzheimer disease biomarkers. Neurology. 2016; 87(5):539-547.
23. Jack CR, Jr., Bennett DA, Blennow K, et al. NIA-AA Research Framework: Towards a Biological Definition of Alzheimer's Disease. Alzheimer's Dement. 2018; 14(4):535-562.
24. de Vos F, Schouten TM, Hafkemeijer A, et al. Combining multiple anatomical MRI measures. improves Alzheimer's disease classification. Hum Brain Mapp. 2016; 37:1920–1929.
25. Wang P, Chen K, Yao L, et al. Multimodal classification of mild cognitive impairment based on partial 598 least squares. J Alzheimers Dis. 2016; 54:359–371.
26. Dimitriadis SI, Liparas D, Tsolaki MN, Alzheimer's Disease Neuroimaging Initiative. Random forest feature selection, fusion and ensemble strategy: combining multiple morphological MRI measures to discriminate among health elderly, MCI, cMCI and Alzheimer's disease patients: from the Alzheimer's disease neuroimaging initiative (ADNI) database. J Neurosci Methods. 2018; 302:14-23.
27. Sarica A, Cerasa A, Quattrone A. Random Forest Algorithm for the Classification of Neuroimaging Data in Alzheimer's Disease: A Systematic Review. Front Aging Neurosci. 2017; 9:329.
28. Clark CM, Schneider JA, Bedell BJ, et al. Use of florbetapir-PET for imaging beta-amyloid pathology. JAMA. 2011; 305:275–83.
29. Palmqvist S, Scholl M, Strandberg O, et al. Earliest accumulation of beta-amyloid occurs within the default-mode network and concurrently affects brain connectivity. Nat Commun. 2017; 8(1):1214.
30. Buckner RL, Snyder AZ, Shannon BJ, et al. Molecular, structural, and functional characterization of Alzheimer's disease: Evidence for a relationship between default activity, amyloid, and memory. J Neurosci. 2005; 25(34):7709-7717.

Legends for illustrations

Figure 1: Illustration of a hypothetical tree in a RF. Decision nodes are represented by rounded rectangles with feature and decision threshold that best separates data into two classes based on training cases, starting from the root node at top. Leaf nodes are represented by the final classification as negative (NEG) or positive (POS).

Figure 2: Illustration of image-processing pipeline using the MINC toolkit. A clinically negative case is shown in (A-F) and a clinically positive case is shown in (G-L). (A,G) Raw PET images with 4 consecutive imaging sequences. (B,H) Averaged and blurred PET image. (C,I) Patient MRI. (D,J) Patient PET registered into template space, showing SUVR on a colour scale with blue indicating lower SUVR and red indicating higher SUVR. (E,K) MRI template. (F,L) Jack mask ROI superimposed on PET image.

Figure 3: Illustration of key regions identified by the RF on a surface projection of the brain: anterior cingulate (yellow), posterior cingulate (blue), precuneus (red), and middle frontal gyrus (green).

Table 1: Summary of measurements from training, test, and entire data set.

Parameter	**Training set**	**Testing set**	**Overall data set**
Number of cases	37	20	57
Sex	19 male, 18 female	12 male, 8 female	31 male, 26 female
Age (min, median, max)	(61, 76, 91)	(57, 76, 88)	(57, 76, 91)
Memory/stroke	26 memory, 11 stroke	12 memory, 8 stroke	38 memory, 19 stroke
White matter hyperintensity [cm^3] (min, median, max)	(8.2, 26.6, 103.7)	(8.4, 26.1, 88.2)	(8.2, 26.3, 103.7)
SUVR (min, median, max)	(1.03, 1.42, 2.49)	(0.68, 1.46, 2.27)	(0.68, 1.44, 2.49)
Clinical read	22 negative, 15 positive	13 negative, 7 positive	35 negative, 22 positive

Table 2: Confusion matrix summarizing classification results from the RF.

		True classification	
		Negative	Positive
Predicted classification	Negative	12	1
	Positive	1	6

Table 3: List of features found most often at the root node in an RF with 10,000 trees trained to classify brain PET scans as positive or negative for amyloid deposition, using 15 randomly selected scans and 20 randomly selected features (SUVR in brain ROIs).

Region	**Number of instances at a root node**
Left posterior cingulate	1039
Left middle frontal gyrus	1038
Left precuneus	857
Right anterior cingulate gyrus	655
Right posterior cingulate	588
Right precuneus	408
Left anterior cingulate gyrus	342
Right gyrus rectus	319
Left gyrus rectus	299
Right middle temporal gyrus	270

Table 4: List of test scans, number of trees in the RF that return a negative or positive decision, and whether the cases are true negative (TN), false negative (FN), false positive (FP), or true positive (TP) using the clinical brain PET read as the gold standard.

Test case	**Number of trees with negative decision**	**Number of trees with positive decision**	**Result**
1	6276	3724	TN
2	2817	7183	TP
3	7904	2096	TN
4	**4183**	**5817**	**FP**
5	8688	1312	TN
6	5246	4754	TN
7	9654	346	TN
8	7572	2428	TN
9	8447	1553	TN
10	2835	7165	TP
11	3181	6819	TP
12	9591	409	TN
13	8730	1270	TN
14	9766	234	TN
15	7907	2093	TN
16	1687	8313	TP
17	3634	6366	TP
18	5023	4977	TN
19	3501	6499	TP
20	**5426**	**4574**	**FN**

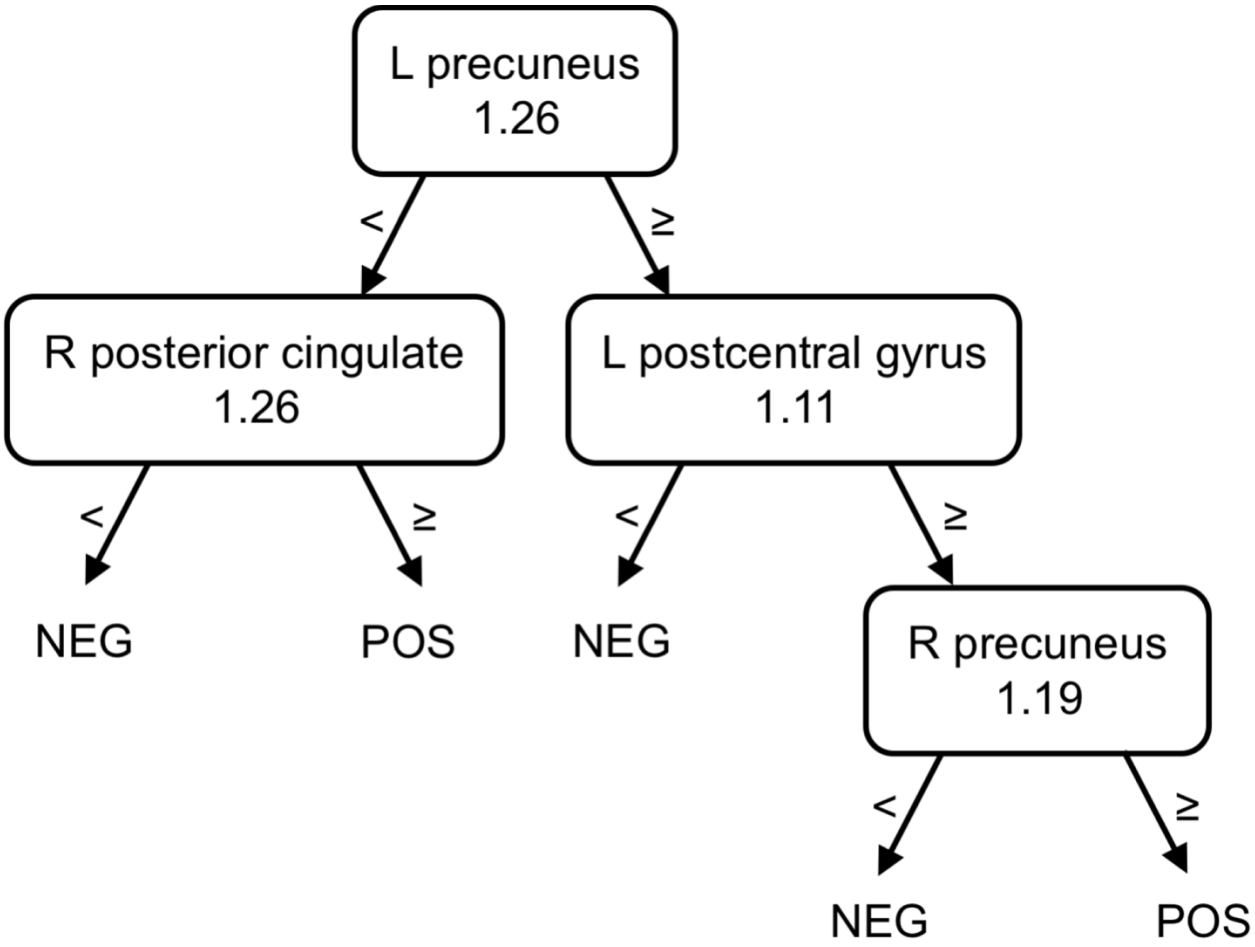
L precuneus
1.26
<
≥
R posterior cingulate
1.26
L postcentral gyrus
1.11
<
≥
<
≥
NEG
POS
NEG
R precuneus
1.19
<
≥
NEG
POS

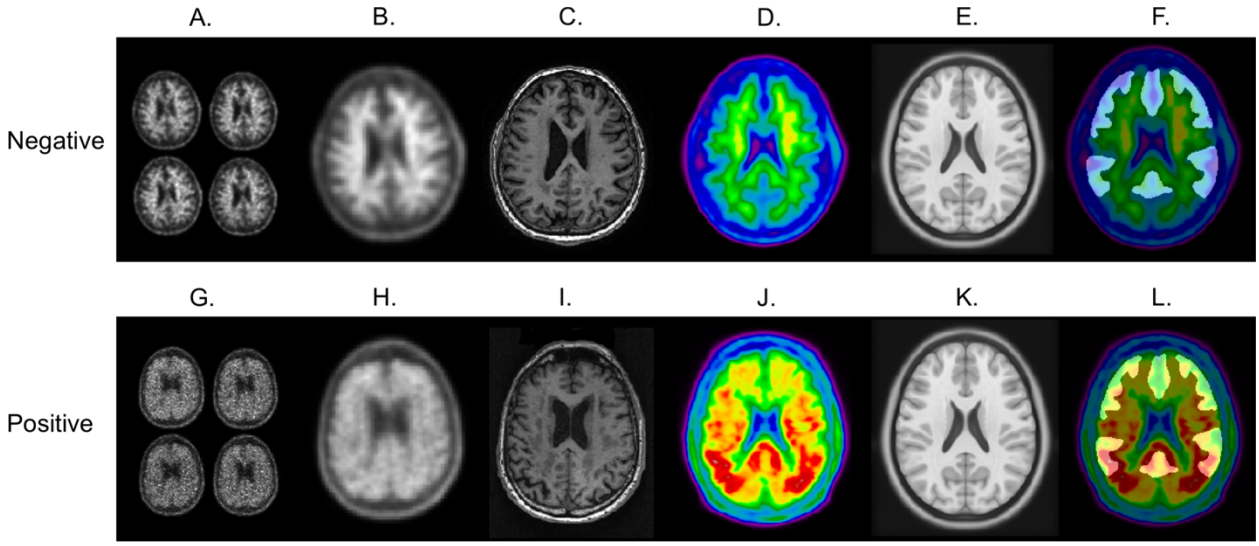
A.
B.
C.
D.
E.
F.
Negative
G.
H.
I.
J.
K.
L.
Positive

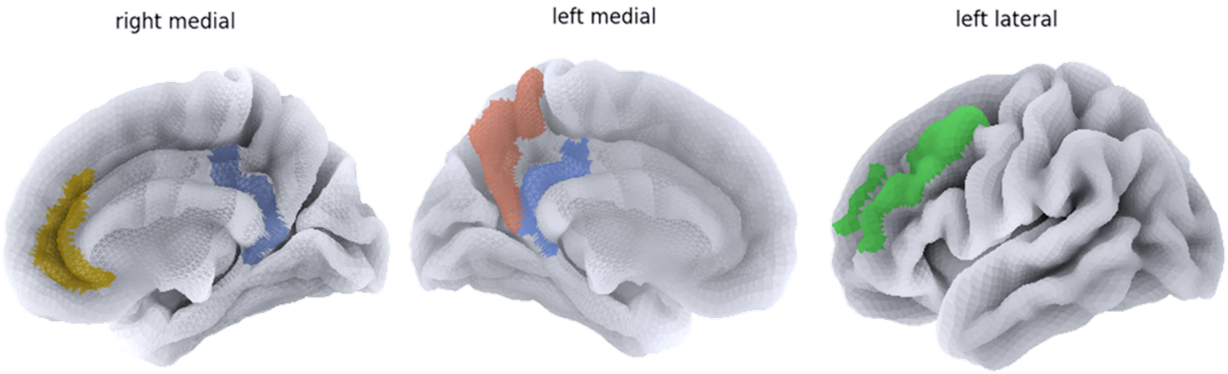
right medial
left medial
left lateral